Broadband quasi-phase-matched second-harmonic generation of ultrashort optical pulses with spectral angular dispersion

Andrew M. Schober, Mathieu Charbonneau-Lefort, and Martin M. Fejer

E. L. Ginzton Laboratory, Stanford University, Stanford, California 94305-4085

Received October 11, 2004; revised manuscript received January 25, 2005; accepted February 16, 2005

Noncollinear quasi-phase matching, in combination with spectral angular dispersion, can be used to broaden the bandwidth of second-harmonic generation (SHG) beyond the bandwidth for collinear, nondispersed interactions. A general theoretical treatment is presented, in addition to a solution that predicts the generated field for the case of a Gaussian input field; a comparison is made between this technique and others available for broadband SHG. An experiment in periodically poled lithium niobate demonstrates SHG of a 138 fs pulse at 1550 nm in a 1 cm length crystal (with a collinear acceptance bandwidth 13 times narrower than the first-harmonic bandwidth) with minimal spectral narrowing.

OCIS codes: 190.7110, 190.4360.

1. INTRODUCTION

Laser gain media capable of short-pulse generation are available over only a small portion of the optical spectrum, whereas applications from spectroscopy to high-field science and optical communications often require pulses in inaccessible spectral regions. Nonlinear frequency conversion of short pulses can fill these spectral regions. To preserve the short-pulse duration, the acceptance bandwidth of a nonlinear interaction must match or exceed the bandwidth of the input pulse. In this paper we discuss ultrashort-pulse second-harmonic generation (SHG).

In addition to a broad bandwidth, high conversion efficiency is also desired. The conversion efficiency of conventional collinear SHG in uniform nonlinear materials is proportional to the square of the interaction length, but the bandwidth is inversely proportional to the same interaction length, resulting in a trade-off between conversion efficiency and bandwidth. Several methods have been demonstrated to reduce or eliminate this trade-off.

In the simplest collinear interactions (type 0 quasi-phase-matched SHG or type I and type II birefringent phase-matched SHG), the bandwidth of SHG is limited by the difference in group velocity between the first-harmonic (FH) and second-harmonic (SH) wave.[1,2] A FH wave packet traveling through a nonlinear medium will lead or lag (depending on the shape of the dispersion curve) the generated SH wave that travels at a different group velocity because of dispersion in the group index of the nonlinear medium. In a crystal longer than a walk-off length (the crystal length that results in a difference in group delay equal to the FH pulse width) this velocity mismatch results in a SH pulse that is significantly longer than the FH input, or in the frequency domain has a significantly narrower bandwidth. Consequently, to preserve the bandwidth of the SH wave, the maximum crystal length is approximately limited to the walk-off length. A reduced mismatch between group velocities of the interacting waves results in a longer maximum interaction length.[2]

Occasionally, nature provides perfect matching of the group velocities of FH and SH waves for a particular pair of frequencies in a nonlinear medium. This is not, in general, the same frequency for which the phase velocities are matched, but with quasi-phase matching (QPM) it is often possible to simultaneously quasi-phase match and group-velocity match a SHG interaction at a particular FH frequency in a given nonlinear material. For example, in lithium niobate, the FH and SH group velocities are matched in a type 0 ($e+e \rightarrow e$) interaction at a FH wavelength near 2.6 μm.[3] This method for group-velocity matching is available only at specific frequencies determined by the dispersion of the nonlinear material and may not be generally applicable across the material's transparency window. Nevertheless, group-velocity-matched SHG has been demonstrated in a variety of materials utilizing both birefringent phase matching and QPM.[4–9]

A more general technique for broadband SHG has been demonstrated through longitudinal patterning of a QPM grating.[10,11] Longitudinal variation of the QPM period provides for localized conversion of the different frequency components of a short pulse at different positions along the propagation axis of a nonlinear device. A distribution of QPM periods allows for a broader distribution of phase-matched frequencies and an increased bandwidth compared with a uniform grating of the same length. The localized frequency conversion in the presence of a difference in group velocity between FH and SH waves results in a chirped SHG transfer function.[2] Consequently, although the SHG of a transform-limited FH pulse that is used with a chirped QPM grating may preserve the band-

0740-3224/05/081699-15/$15.00

width, the pulse width will not be preserved. The resulting chirped SH pulse may, however, be compressed to the transform limit by use of a dispersive element.

A fourth technique, the topic of this paper, makes use of spectral angular dispersion in a noncollinear geometry to broaden the bandwidth of ultrashort-pulse SHG. In a critically phase-matched continuous-wave (cw) interaction, the phase-matching wavelength depends linearly on the angular detuning of the nonlinear crystal. Decomposing a broadband FH field into plane waves, we find that angular dispersion programs frequency-dependent angular detuning into the FH field, effectively broadening the acceptance bandwidth. The idea of using spectral angular dispersion to broaden the phase-matching bandwidth was first proposed in the 1970s to broaden the bandwidth of cw SHG[12–14] and was later suggested for short-pulse applications.[15,16] Variations of this technique have been discussed theoretically[17,18] and verified experimentally for both broadly tunable cw SHG[19,20] and for ultrashort-pulse generation[16,21,22] in birefringently phase-matched nonlinear materials. Angular dispersion applied to pulsed SHG in quasi-phase-matched materials was first presented in Ref. 23, including calculations for the device configuration specific to periodically poled lithium niobate (PPLN), which we experimentally verify in this study. In addition, we expand on established theory to include a detailed discussion of the conversion efficiency and limitations imposed by diffraction and spatial walk-off.

The remainder of this paper is devoted to the demonstration and analysis of broadband SHG of ultrashort optical pulses in the presence of spectral angular dispersion. In Section 2 we describe a frequency-domain technique of using spectral angular dispersion in a noncollinear geometry to compensate for material dispersion in SHG. This technique is equivalent to the matching of the FH and SH group velocities in the time domain using a tilted pulse front, as illustrated in Section 3. In Section 4 we present an experimental demonstration of broadband SHG with spectral angular dispersion. In Section 4 we demonstrate group-velocity-matched SHG in PPLN, motivating the development of a deeper theoretical understanding of the conversion efficiency in this noncollinear geometry. It is this theoretical treatment that occupies the later sections of this paper.

In Section 5 we derive the scalar wave equations for noncollinear SHG assuming an undepleted pump and including the effects of dispersion, diffraction, and spatial walk-off. In Section 6 we present a general solution to these equations, and in Section 7 we discuss the solution in the particular case of a Gaussian FH field envelope. In Section 8 we describe the effects that group-velocity dispersion (GVD) and spatial walk-off have on the SH field predicted by the results presented in Section 7. In Section 9 we present the conversion efficiency in the limit of negligible spatial walk-off and diffractive effects and compare the resulting expression to the efficiency for other techniques for ultrashort-pulse SHG. In Section 10 we discuss the scaling of conversion efficiency with regard to focusing and spatial walk-off and the trade-offs between beam quality and size and conversion efficiency that result from tight focusing or increased phase-matching angle. Finally, in Section 11 we summarize the results of this paper.

2. FREQUENCY-DOMAIN DESCRIPTION

Consider a FH plane wave with wave vector $\mathbf{k}(\omega)$ and frequency ω generating a SH plane wave with wave vector $\mathbf{k}(2\omega)$ and frequency 2ω inside a QPM grating with grating vector $\mathbf{K}_g$. The grating vector is in a direction normal to the QPM grating lines and has magnitude $K_g=2\pi/\Lambda$, where Λ is the QPM period.[1] This geometry is shown schematically in Fig. 1. The angle ϕ is measured between $\mathbf{k}(\omega)$ and $\mathbf{K}_g$, and θ is measured between $\mathbf{k}(\omega)$ and $\mathbf{k}(2\omega)$. The wave-vector mismatch is defined as the vector sum $\mathbf{\Delta k}(\omega)=2\mathbf{k}(\omega)-\mathbf{k}(2\omega)+\mathbf{K}_g$. The interaction is quasi-phase matched at frequency ω when $\mathbf{\Delta k}(\omega)=0$. QPM provides more flexibility than birefringent phase matching since the magnitude and direction of $\mathbf{K}_g$ may be engineered for a variety of applications.[1] When a collinear geometry is used, $\mathbf{k}(\omega)$, $\mathbf{k}(2\omega)$, and $\mathbf{K}_g$ are parallel vectors but QPM has similar engineering advantages regarding noncollinear interactions.

The magnitudes of $\mathbf{k}(\omega)$ and $\mathbf{k}(2\omega)$ change with frequency because of dispersion in the refractive index of the nonlinear material; but in the presence of spectral angular dispersion, the directions of the FH and SH wave vectors may also vary with frequency, and the angles ϕ and θ are frequency dependent. If the angles ϕ and θ are appropriate functions of frequency, the spectral angular dispersion may offset the effects of material dispersion, broadening the acceptance bandwidth of a nonlinear device.

The SHG interaction is quasi-phase matched when $\mathbf{\Delta k}(\omega)=0$ or the triangle formed by the vectors $2\mathbf{k}(\omega)$, $\mathbf{k}(2\omega)$, and $\mathbf{K}_g$ is closed. Using the law of cosines, we can write this condition as[23]

$$\cos\phi=-\frac{K_g^2+4[k(\omega)]^2-[k(2\omega)]^2}{4K_g k(\omega)}, \tag{1}$$

where $k(\omega)$ is the magnitude of $\mathbf{k}(\omega)$, and similar notation is used for the SH wave vector and the QPM grating wave vector. Suppose the phase-matching condition in Eq. (1) is

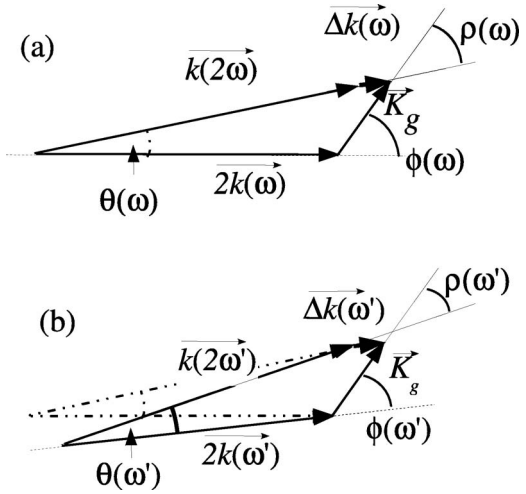

Fig. 1. Frequency-domain picture of plane-wave noncollinear QPM SHG. (a) QPM condition at frequency ω. (b) QPM condition at frequency ω' (solid lines), where the dotted lines indicate the QPM condition at ω. If θ' and ϕ' are chosen appropriately, $\mathbf{\Delta k}(\omega)=\mathbf{\Delta k}(\omega')$ and angular dispersion compensates material dispersion to maintain a constant phase mismatch.

met at the FH carrier frequency ω_1 with angles ϕ_0 and θ_0. If we differentiate Eq. (1) with respect to frequency, then we find that, to first order in ω, the spectral angular dispersion required to maintain QPM is

$$\left.\frac{\partial\phi}{\partial\omega}\right|_{\omega_1} = \frac{\delta\nu}{k(\omega_1)\theta_0}, \tag{2}$$

where $\delta\nu$ is the group-velocity mismatch parameter defined as

$$\delta\nu = \left.\frac{\partial k(\omega)}{\partial\omega}\right|_{\omega_1} - \left.\frac{\partial k(\omega)}{\partial\omega}\right|_{\omega_2}, \tag{3}$$

where we assumed that $\theta_0 \ll 1$ (an exact expression for all angles may be found in Ref. 23). A similar analysis gives the resulting angular dispersion of the SH wave in this dispersion-compensated geometry:

$$\left.\frac{\partial\rho}{\partial\omega}\right|_{\omega_2} = \frac{\delta\nu}{k(2\omega_1)\theta_0}, \tag{4}$$

where $\rho = \pi - \theta - \phi$ is the angle measured between vectors $\mathbf{k}(2\omega)$ and $\mathbf{K}_g$.

3. TIME-DOMAIN DESCRIPTION

In Section 2 we showed that for plane waves, QPM can be maintained over a broad tuning range by introducing spectral angular dispersion as the frequency of a FH plane wave changes. Since an ultrashort pulse is a coherent superposition of monochromatic plane waves with a broad optical spectrum, spectral angular dispersion can also broaden the bandwidth for the SHG of a short optical pulse.

In the time domain, angular dispersion manifests itself as a tilted pulse front.[24] This situation is shown schematically in Fig. 2. Consider at time $t=0$, a FH field (solid outline) at the origin in the x–z plane and propagating in the z direction. It generates some SH field (shaded gray) with approximately the same spatiotemporal envelope. After a time t, the FH field envelope has traveled a distance $u_1 t$ in the z direction, where u_1 is the FH group velocity, and u_i is defined as

$$\frac{1}{u_i} = \left.\frac{\partial k}{\partial\omega}\right|_{\omega_i} \tag{5}$$

for the FH ($i=1$) and SH ($i=2$) fields. The SH field envelope moves a distance $u_2 t$ at a small angle θ_0 (determined by the phase-matching condition) relative to the FH field direction, with $u_2 = (\partial k_2/\partial\omega_2)^{-1}$ equal to the SH group velocity. Taking the tilt angle of the pulse front to be ψ, then the two fields have maximum overlap if θ_0 is chosen such that the position of the centroid of the SH field lies along the tilted pulse front of the SH field. Since the pulse-front tilt is related to the angular dispersion according to[24]

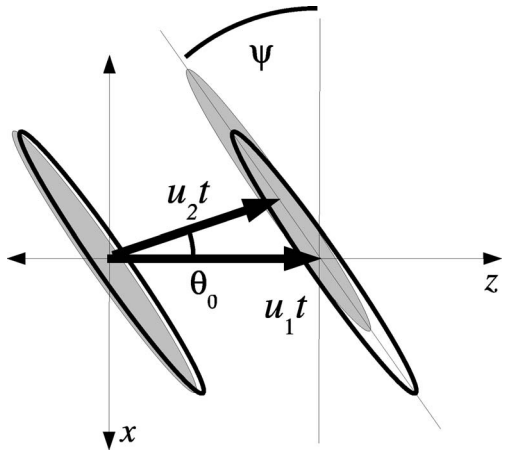

Fig. 2. Time-domain picture of tilted pulse-front group-velocity-matched SHG. The solid outline indicates the FH envelope; the gray shaded area indicates the SH envelope. With appropriately chosen pulse-front tilt angle ψ, the field overlap is maintained with propagation and the group velocities are effectively matched. The angle ψ is related to the spectral angular dispersion through Eq. (6).

$$\psi = -\arctan\left(k_1 u_1 \left.\frac{\partial\phi}{\partial\omega}\right|_{\omega_1}\right), \tag{6}$$

a simple geometric analysis returns the same result as in Eq. (2).

4. EXPERIMENT

We demonstrate here type 0 quasi-phase-matched SHG using spectral angular dispersion to compensate for group-velocity mismatch (GVM). Figure 3(a) shows a schematic diagram of the experimental setup. FH light is incident on a diffraction grating that imposes the requisite spectral angular dispersion. The diffraction grating is then imaged into the center of a PPLN crystal so that the different frequency components of the FH field overlap in space inside the nonlinear crystal. The residual FH is dumped, and the SH is collected and reimaged onto a second diffraction grating, which compensates the spectral angular dispersion of the SH light. Figure 3(b) shows a more detailed view of the SHG interaction, where the poling lines of the QPM grating and the noncollinear interaction can be more clearly visualized.

Our experiment uses transform-limited FH pulses at 138 fs in a full width at half-maximum (FWHM) duration at a wavelength of 1550 nm in a 1 cm long PPLN crystal, with 25 nm of FH bandwidth. At 1550 nm, the walk-off parameter has a value of $\delta\nu = -0.314$ ps/mm, and the collinear SHG bandwidth of a 1 cm grating is 0.56 nm (FWHM) at the SH wavelength. The FH pulses are generated with a Spectra-Physics Opal synchronously pumped optical parametric oscillator operating at a wavelength of 1550 nm, pumped by a Spectra-Physics Tsunami mode-locked Ti:sapphire laser. Pulses are 0.58 nJ in energy and are delivered at a repetition frequency of 82 MHz. The FH is dispersed using a diffraction grating with 400 lines/mm at an incident angle of 21 deg to give an angular dispersion of 1.84 radμm in free space. When the

beam is imaged into the PPLN crystal with unit magnification, the angular dispersion is 0.86 rad/μm inside the crystal.

The PPLN crystal is 1 cm in length, with a poling period of 9.256 μm, or 50% of the collinear phase-matching period. The duty cycle was measured to be 25.5% (as compared with the ideal 50%), resulting in an effective nonlinear coefficient[2] of 12.15 pm/V. The vector phase-matching condition requires an angle of 60.96 deg between the FH beam and the grating wave vector. The poling lines of our PPLN device are at 60 deg relative to the input facet, allowing near-normal incidence to the PPLN crystal. The phase-matching condition calls for an angle between FH and SH waves of 1.92 deg, which, according to Eq. (34), matches the spectral angular dispersion required for group-velocity matching.

The diffraction grating is reimaged at the center of the PPLN crystal so that the spectral components of the FH beam, although propagating at different angles, overlap in space inside the nonlinear crystal. The beam is focused elliptically using cylindrical lenses to achieve a spot 530 μm wide ($1/e^2$ intensity full width) in the x (dispersed) dimension and 180 μm in the y dimension. The SH is then collected, and the beam waist (located in the center of the PPLN crystal) is reimaged onto a diffraction grating with 830 lines/mm at an incident angle of 76.6 deg where the spectral angular dispersion of the SH field is compensated. When we use the simple imaging system shown in Fig. 3, care must be taken to minimize spatial phase distortions due to the imaging system,[15] which can result in spatial chirp if the lenses are not sufficiently placed in the far field. (We use lenses with a 15 cm long

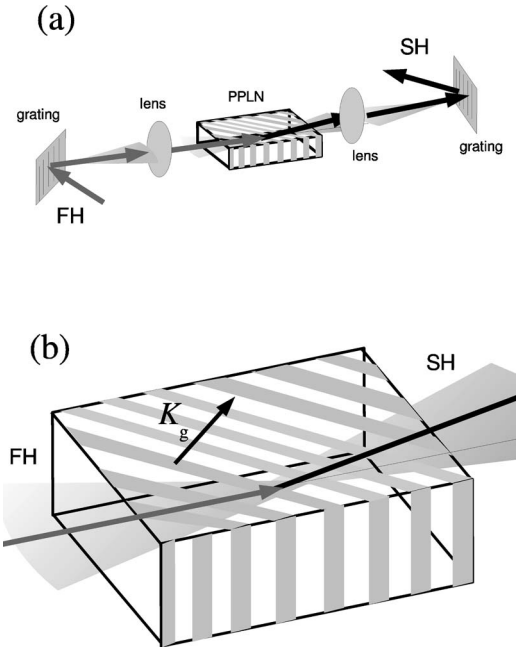

Fig. 3. Schematic diagram of the PPLN experiment with spectral angular dispersion. (a) FH light incident on a diffraction grating acquires spectral angular dispersion. A lens images this spot into the PPLN crystal where SH light is generated. This SH is then reimaged onto an output diffraction grating where the spectral angular dispersion is undone. (b) A closeup view of the SHG interaction illustrating the noncollinear interaction in a tilted QPM grating.

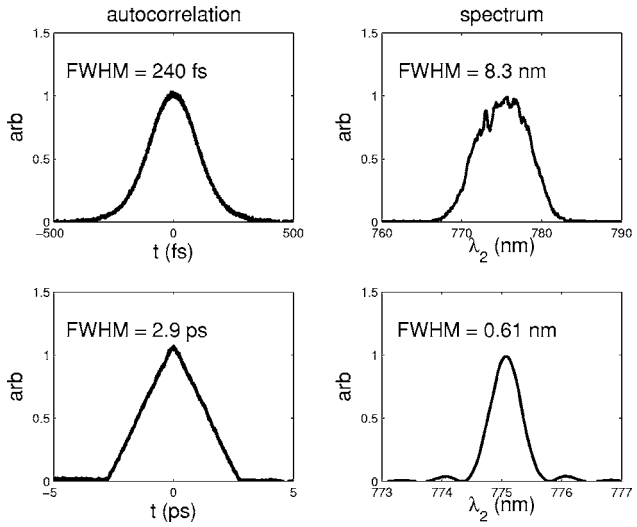

Fig. 4. Results of SHG with spectral angular dispersion in PPLN. Autocorrelation (left) and spectrum (right) of tilted pulse-front SHG (top) and collinear SHG in an identical length crystal in the presence of group-velocity walk-off (bottom). With spectral angular dispersion, the measured autocorrelation has a FWHM of 240 fs and a spectral FWHM of 8.3 nm, nearly 14 times broader than the spectrum of collinear SHG in a crystal of identical length.

focal length, placed 30 cm from the diffraction grating and 30 cm from the PPLN crystal.) Use of a telescope as described by Martinez in Ref. 15 would eliminate the spatial phase distortions present in a single-lens system.

The resulting SH is then analyzed using an autocorrelator and an optical spectrum analyzer. The measurement results are displayed in Fig. 4. For comparison, we also show the measured spectrum and autocorrelation for an identical-length crystal in a traditional collinear orientation, in which the effects of GVM dominate the SHG output. The bandwidth in the noncollinear case is 8.3 nm (FWHM) and is more than 14 times the group-velocity-limited bandwidth of the collinear interaction. Ignoring any bandwidth limitations from SHG, the expected SH bandwidth from FH pulses with a bandwidth of 25 nm is calculated at 9.3 nm (assuming Gaussian FH pulses), and our experiment demonstrates 89% of this maximum bandwidth.

The output SH pulse is 170 fs (FWHM, calculated from the autocorrelation assuming a Gaussian pulse shape) in duration, approximately 1.5 times the transform limit indicating some residual spectral phase on the SH pulses. Diffraction gratings impose not only linear spectral angular dispersion, but higher-order angular dispersion as well onto the FH and SH fields. When the linear spectral angular dispersion is compensated, the higher-order dispersion is not necessarily compensated simultaneously, resulting in SH output with spatially varying frequency chirp. (A discussion of the first-order angular dispersion resulting from the reflection of a short optical pulse from a diffraction grating may be found in Ref. 24, Section 1.5, and a generalization to higher-order dispersion is straightforward.) The magnitude of the higher-order spectral angular dispersion can readily be calculated if the diffraction grating line spacing and the incident angles are known. For the experiment reported in Section 4, the qua-

dratic phase difference across the bandwidth of the SH pulse evaluated at the beam waist is approximately equal to π and is of the correct magnitude to approximately account for the measured difference in pulse duration from the ideal transform-limited case.

The measured conversion efficiency with a FH pulse energy of 0.58 nJ is 6.7% (SH energy of 38.7 pJ). The undepleted pump conversion efficiency for near-field Gaussian beams with FH pulse energy U_1 and a nonlinear coefficient d_m is given by[2]

$$\eta = \frac{2\sqrt{2\pi}d_m^2}{\epsilon_0 c n_2 n_1^2 \lambda_1^2}\frac{U_1 L^2}{w_x w_y \tau_0}, \tag{7}$$

where n_i is the refractive index at the FH ($i=1$) and SH ($i=2$) wavelengths, λ_1 is the FH vacuum wavelength, and L is the interaction length. The FH field is assumed to be a Gaussian field in space and time, with a $1/e$ intensity half-width duration of τ_0 and a beam width equal to w_x and w_y (also $1/e$ intensity half-width) in the transverse x and y dimensions, respectively. If we compute the energy conversion efficiency using the measured beam size of $w_x = 187\ \mu$m ($1/e^2$ full width of 530 μm) and $w_y = 64\ \mu$m ($1/e^2$ full width of 180 μm) and a pulse duration of 138 fs ($\tau_0 = 84$ fs) in our experiment, we find that an estimate for the normalized conversion efficiency is $\eta_0/U_1L^2 = 108\%/(\text{nJ/cm}^2)$; with a 1 cm crystal length and 0.58 nJ of pump energy, this predicts conversion well into the pump depletion regime.

It is clear that the simplified plane-wave analysis does not accurately predict the conversion efficiency of noncollinear SHG with angular dispersion; in Sections 5–10 we present a theory that more accurately predicts the conversion efficiency. In addition, our model includes the effects of GVD, diffraction, and spatial walk-off. The influence of these effects on noncollinear, group-velocity-matched SHG is discussed in detail.

5. THEORETICAL MODEL

SHG of a strongly tilted pulse in a noncollinear geometry departs from a plane-wave description in several ways. Perhaps the most obvious is the influence of spatial walk-off, where the generated SH field envelope walks off of the generating FH beam because of the noncollinear nature of the interaction. In a more subtle way, the pulse-front tilt also has a profound influence as a tilted pulse is affected by diffraction more than an untilted pulse of the same beam width.

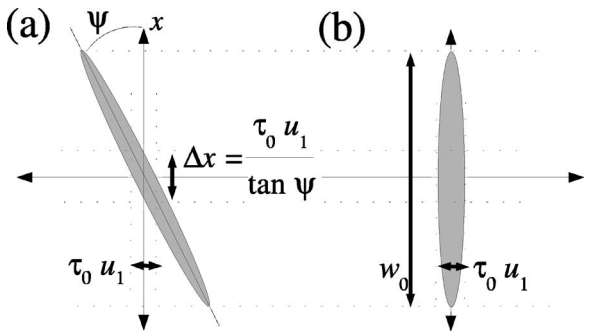

Fig. 5. Field envelope of a tilted pulse with (a) tilt angle ψ and (b) an untilted pulse. The width Δx that determines the importance of diffraction may be much less than the beam width w_0 for a tilted pulse. Such a tilted field will experience diffractive effects with a characteristic length $L_R' = k_0 \Delta x^2$ rather than the diffraction length $L_R = k_0 w_0^2$ determined by the beam width w_0.

As illustrated in Fig. 5, a field with beam width w_0 and temporal pulse width τ_0 subject to a large pulse tilt has a cross section $\Delta x \ll w_0$. In Fig. 5 we show field envelopes for a tilted pulse with tilt angle ψ [Fig. 5(a)] and an untilted pulse [Fig. 5(b)]. In both cases, the envelope propagates normal to the x axis. The diffraction length for a beam of width w_0 is $L_R = k w_0^2$ where $k = 2\pi n/\lambda$ is the magnitude of the wave vector, given in terms of the refractive index n and the vacuum wavelength λ. However, diffraction of a tilted optical pulse has a characteristic length of $L_R' = k\Delta x^2 \ll L_R$. Here we present a model that accounts for this difference and examine its effects on the generation of strongly tilted pulses.

To derive the equations that govern noncollinear SHG with spectral angular dispersion, we consider undepleted pump SHG in a nonlinear, nonmagnetic dielectric with propagation direction z and variation in one transverse dimension x. The frequency-domain coupled scalar wave equations are[2]

$$\frac{\partial^2 \hat{E}_1(z,x,\omega)}{\partial z^2} + \frac{\partial^2 \hat{E}_1(z,x,\omega)}{\partial x^2} + k^2(\omega)\hat{E}_1(z,x,\omega) = 0, \tag{8}$$

$$\frac{\partial^2 \hat{E}_2(z,x,\omega)}{\partial z^2} + \frac{\partial^2 \hat{E}_2(z,x,\omega)}{\partial x^2} + k^2(\omega)\hat{E}_2(z,x,\omega) = -\mu_0 \omega_2^2 \hat{P}_{\mathrm{NL}}(z,x,\omega), \tag{9}$$

where $k^2(\omega) = \omega^2 \epsilon(\omega)/c^2$ and $\hat{P}_{\mathrm{NL}}(z,x,\omega)$ is the nonlinear polarization. Subscripts 1 and 2 refer to the FH and SH field, respectively. It is convenient to define an electric field envelope function $B_i(z,x,t)$:

$$E_i(z,x,t) = E_0 B_i(z,x,t)\exp(i\omega_i t - ik_{z,i}z - ik_{x,i}x), \tag{10}$$

where $k_{z,i}$ and $k_{x,i}$ are the z and x components, respectively, of the wave vector $\mathbf{k}(\omega_i)$ evaluated at the carrier frequency ω_i. We explicitly factored out the FH field amplitude E_0, so that $B_i(z,x,t)$ is dimensionless and the FH envelope has unit amplitude. The magnitude of the wave vector at the carrier frequency is k_i and is related to the components by $k_i^2 = k_{z,i}^2 + k_{x,i}^2$. The corresponding frequency-domain electric field $\hat{E}_i(z,x,\omega)$ is related to the Fourier transform $\hat{B}_i(z,x,\Omega_i)$ of this time-domain envelope as

$$\hat{E}_i(z,x,\omega) = E_0 \hat{B}_i(z,x,\Omega_i)\exp(-ik_{z,i}z - ik_{x,i}x), \tag{11}$$

where $\Omega_i = \omega - \omega_i$ is the frequency detuning. To examine the effect of dispersive terms, we expand $k^2(\omega)$ in a Taylor series around the carrier frequency for the respective fields:

$$k^2(\omega) \approx k_i^2 + 2k_i\frac{1}{u_i}\Omega_i + \frac{1}{u_i^2}\Omega_i^2 + k_i\beta_i\Omega_i^2, \tag{12}$$

where k_i is the magnitude of the wave vector at the carrier frequency ω_i, u_i is the group velocity defined in Eq. (5), and β_i is the GVD coefficient defined as

$$\beta_i = \left.\frac{\partial^2 k}{\partial \omega^2}\right|_{\omega_i}. \tag{13}$$

For periodic nonlinear media, we assume that the nonlinear coefficient distribution $d(z,x)$ is dominated by a uniform grating vector with z and x components designated by $K_{g,z}$ and $K_{g,x}$, respectively, and we find that the nonlinear coefficient distribution is given by

$$d(z,x) \approx d_m \exp(iK_{g,z}z + iK_{g,x}x), \tag{14}$$

where d_m is the Fourier component of a QPM grating of order m. The nonlinear polarization is defined as

$$P_{\mathrm{NL}}(z,x,t) = \epsilon_0 d(z,x)E_1^2(z,x,t). \tag{15}$$

Substituting the above expansions and envelope definitions into the coupled equations and Fourier transforming, we find the time-domain form of the coupled envelope equations including dispersive terms to second order. In the following equations [Eqs. (16) and (17)], for simplicity we drop the arguments from the field envelopes $B_i = B_i(z,x,t)$ and orient our coordinate system along the direction of propagation of the FH wave, such that $k_{x,1}=0$ and $k_{z,1}=k_1$.

$$\frac{\partial^2 B_1}{\partial z^2} - 2ik_1\frac{\partial B_1}{\partial z} + \frac{\partial^2 B_1}{\partial x^2} - 2i\frac{k_1}{u_1}\frac{\partial B_1}{\partial t} - \frac{1}{u_1^2}\frac{\partial^2 B_1}{\partial t^2} - k_1\beta_1\frac{\partial^2 B_1}{\partial t^2} = 0, \tag{16}$$

$$\frac{\partial^2 B_2}{\partial z^2} - 2ik_{z,2}\frac{\partial B_2}{\partial z} + \frac{\partial^2 B_2}{\partial x^2} - 2ik_{x,2}\frac{\partial B_2}{\partial x} - 2i\frac{k_{z,2}}{u_2}\frac{\partial B_2}{\partial t} - \frac{1}{u_2^2}\frac{\partial^2 B_2}{\partial t^2} - k_2\beta_2\frac{\partial^2 B_2}{\partial t^2} = -\frac{4\omega_1^2 d_m E_0}{c^2}B_1^2\exp(-i\Delta k_z z - i\Delta k_x x). \tag{17}$$

The z component of the wave-vector mismatch $\mathbf{\Delta k} = 2\mathbf{k}_1 - \mathbf{k}_2 + \mathbf{K}_g$ is defined as $\Delta k_z = 2k_1 - k_{z,2} + K_{g,z}$, and the x component is $\Delta k_x = -k_{x,2} + K_{g,x}$. Hereafter we assume that the interaction is quasi-phase matched at the carrier frequencies, i.e., $\Delta k_z = 0$ and $\Delta k_x = 0$.

It is convenient to change coordinate systems to a reference frame that moves along with the FH field at the group velocity u_1. We define a new time coordinate $T = t - z/u_1$, which is the time delay relative to the center of a freely propagating field envelope at the FH group velocity. The resulting coupled equations, in the limit of a slowly varying field envelope, are

$$i\frac{\partial B_1}{\partial \bar{z}} - \frac{1}{2}\frac{L}{L_{R,1}}\frac{\partial^2 B_1}{\partial \bar{x}^2} + \frac{L}{L_{D,1}}\frac{\partial^2 B_1}{\partial \bar{T}^2} = 0, \tag{18}$$

$$i\frac{\partial B_2}{\partial \bar{z}} - i\frac{L}{L_g}\frac{\partial B_2}{\partial \bar{T}} + i\frac{L}{L_a}\frac{\partial B_2}{\partial \bar{x}} - \frac{1}{2}\frac{L}{L_{R,2}}\frac{\partial^2 B_2}{\partial \bar{x}^2} + \frac{L}{L_{D,2}}\frac{\partial^2 B_2}{\partial \bar{T}^2} - c_2 B_1^2 = 0, \tag{19}$$

where the coupling coefficient is

$$c_2 = \frac{2\pi d_m E_0 L}{n_2 \lambda_1}, \tag{20}$$

and the normalized coordinates $\bar{z} = z/L$, $\bar{x} = x/w_0$, and $\bar{T} = T/\tau_0$ are defined relative to the interaction length L, the characteristic beam size w_0, and the temporal pulsewidth τ_0. Note that both spatial and temporal walk-off terms appear only in the equation for the SH field, indicating that our chosen reference frame is along the direction of propagation of the FH field ($k_{x,1}=0$) and moves at the FH group velocity.

The coupled equations are now clearly cast in terms of characteristic lengths: the aperture length

$$L_a = \frac{w_0}{\tan(\theta_0)}, \tag{21}$$

where $\tan(\theta_0) = k_{x,2}/k_{z,2}$; the group-velocity walk-off length

$$L_g = \frac{\tau_0}{\delta\nu}; \tag{22}$$

the Rayleigh length

$$L_{R,i} = k_i w_0^2; \tag{23}$$

and the dispersion length

$$L_{D,i} = \frac{2\tau_0^2}{\beta_i}. \tag{24}$$

Equations (18) and (19) are normalized coupled equations for the SHG of short pulses in a noncollinear geometry, allowing for spatial walk-off, diffraction, temporal walk-off, and GVD. To include the effects of spectral angular dispersion, we define an angular dispersion parameter for the FH wave[24] as

$$\gamma_1 = \frac{k_1 w_0}{\tau_0}\left.\frac{\partial \phi(\omega)}{\partial \omega}\right|_{\omega_1}, \tag{25}$$

which is also related to the pulse-front tilt angle ψ through

$$\tan\psi = -\frac{\tau_0 u_1}{w_0}\gamma_1, \tag{26}$$

according to Eq. (6).

A field envelope $B_i(\bar{z},\bar{x},\bar{T})$ that acquires spectral angular dispersion γ_1 undergoes a transformation to a tilted pulse-front envelope where the time delay of the field at transverse position $\bar{x}$ is advanced or retarded by an amount $\gamma_1\bar{x}$, and the field transforms accordingly: $B_i(\bar{z},\bar{x},\bar{T}) \rightarrow B_i(\bar{z},\bar{x},\bar{T}-\gamma_1\bar{x})$.[24]

A strongly tilted ($|\gamma_1| \gg 1$) field envelope diffracts quite differently than an untilted field envelope, and, as illus-

trated in Fig. 5, a tilted pulse may be influenced by diffraction even over distances much smaller than the Rayleigh length set by the beam width w_0. A tilted field envelope in a Cartesian coordinate system can be represented by an untilted field in a tilted coordinate plane. We show that this transformation introduces an angular dispersion term into the coupled equations, which, while physically nonintuitive, allows a simple mathematical treatment. The advantage of such a transformation becomes apparent as our intuition returns for effects such as diffraction and dispersion. In this transformation, diffraction is separated into beam diffraction (determined by the beam width w_0) and diffraction due to pulse-front tilt that we treat as an effective GVD. In this formulation, we need only consider new effective GVD, group-velocity walk-off, and diffraction coefficients.

A transformation of Eqs. (18) and (19) from coordinates $(\bar{z},\bar{x},\bar{T})$ to the tilted coordinates $(\bar{z},\bar{x},\bar{\tau}=\bar{T}-\gamma_1\bar{x})$ involves a transformation of the differential operators

$$\frac{\partial}{\partial\bar{x}} \rightarrow \frac{\partial}{\partial\bar{x}} - \gamma_1\frac{\partial}{\partial\bar{\tau}}, \tag{27}$$

$$\frac{\partial}{\partial\bar{T}} \rightarrow \frac{\partial}{\partial\bar{\tau}}, \tag{28}$$

$$\frac{\partial^2}{\partial\bar{x}^2} \rightarrow \frac{\partial^2}{\partial\bar{x}^2} + \gamma_1^2\frac{\partial^2}{\partial\bar{\tau}^2} - 2\gamma_1\frac{\partial^2}{\partial\bar{x}\,\partial\bar{\tau}}, \tag{29}$$

$$\frac{\partial^2}{\partial\bar{T}^2} \rightarrow \frac{\partial^2}{\partial\bar{\tau}^2} \tag{30}$$

and results in the coupled-wave equations

$$i\frac{\partial B_1}{\partial\bar{z}} - \frac{1}{2}\frac{L}{L_{R,1}}\frac{\partial^2 B_1}{\partial\bar{x}^2} + \frac{L}{L'_{D,1}}\frac{\partial^2 B_1}{\partial\bar{\tau}^2} + \gamma_1\frac{L}{L_{R,1}}\frac{\partial^2 B_1}{\partial\bar{x}\,\partial\bar{\tau}} = 0, \tag{31}$$

$$i\frac{\partial B_2}{\partial\bar{z}} - i\left(\frac{L}{L_g} + \gamma_1\frac{L}{L_a}\right)\frac{\partial B_2}{\partial\bar{\tau}} + i\frac{L}{L_a}\frac{\partial B_2}{\partial\bar{x}} - \frac{1}{2}\frac{L}{L_{R,2}}\frac{\partial^2 B_2}{\partial\bar{x}^2} + \frac{L}{L'_{D,2}}\frac{\partial^2 B_2}{\partial\bar{\tau}^2} + \gamma_1\frac{L}{L_{R,2}}\frac{\partial^2 B_2}{\partial\bar{x}\,\partial\bar{\tau}} - c_2 B_1^2 = 0. \tag{32}$$

The time variable $\bar{\tau}$ may be understood as the normalized time delay relative to the time delay of the envelope center $(\gamma_1\bar{x})$ for each position $\bar{x}$. The coefficients for the $\bar{x}$ derivatives do not change, but the coefficients for time derivatives do change; and there appears a mixed angular dispersion term with coefficients $2\gamma_1 L/L_{R,i}$. The diffraction of tilted pulses in this transformation results in an effective dispersion length given by

$$\frac{1}{L'_{D,i}} = \frac{1}{L_{D,i}} - \frac{1}{2}\frac{\gamma_1^2}{L_{R,i}}. \tag{33}$$

The effective dispersion is a combination of GVD and effective temporal dispersion introduced by the diffraction of a tilted pulse front. The diffraction of the tilted pulse front as shown in Fig. 5 is now separated from the diffraction of the beam and characterized as an effective GVD. The field envelopes in Eqs. (31) and (32) are untilted since we have instead tilted the coordinate system. Our intuition again returns regarding diffraction and dispersion, and we can ignore the effects in Eqs. (31) and (32) term by term when the interaction length L is much less than the corresponding characteristic length. We will show that the added complication introduced by the mixed angular dispersion term $(\partial^2/\partial\bar{x}\,\partial\bar{\tau})$ poses little difficulty in the analysis.

If we choose the pulse-front tilt so that $\gamma_1=-L_a/L_g$, the GVM term is eliminated from Eq. (32). Recalling the definition of γ_1 from Eq. (25), we find a simple relation between the spectral angular dispersion and the phase-matching angle between the FH and SH waves:

$$\left.\frac{\partial\phi(\omega)}{\partial\omega}\right|_{\omega_1} = \frac{\delta\nu}{k_1\theta_0}, \tag{34}$$

which is identical to that given in Eq. (2). For the remainder of this paper, we assume that $\gamma_1=-L_a/L_g$ and thus that the effects of GVM may be neglected.

For a particular QPM grating and choice of FH and SH wavelengths, the phase-matching angle θ_0 is fixed and, through Eq. (34), so is the required spectral angular dispersion. If the collinear limit is approached $(\theta_0\rightarrow 0)$, we find that the spectral angular dispersion required for group-velocity matching becomes very large. Conversely, if the untilted limit is approached $(\partial\phi/\partial\omega\rightarrow 0)$, the phase-matching angle required for group-velocity matching must also be very large, and the result will be that a large beam or a short interaction length will be required to avoid the effects of spatial walk-off.

To take advantage of a long interaction length, a small phase-matching angle is typically desired, and γ_1 is large. Consequently, the dispersive terms in Eqs. (31) and (32) cannot, in general, be ignored even if the crystal is shorter than the material dispersion length, since an effective dispersion arises that may be many times the magnitude of the conventional GVD.

6. GENERAL SOLUTIONS

In this section we solve Eqs. (31) and (32) in the limit of an undepleted pump and ignoring beam diffraction. These equations can be more easily solved in the temporal- and spatial-frequency domains, so we Fourier transform the coupled equations using the transform pair

$$F(x,\tau) = \frac{1}{2\pi}\int_{-\infty}^{\infty}\int_{-\infty}^{\infty}\hat{F}(\xi,\Omega)\exp(i\Omega\tau - i\xi x)\mathrm{d}\xi\mathrm{d}\Omega, \tag{35}$$

$$\hat{F}(\xi,\Omega) = \frac{1}{2\pi}\int_{-\infty}^{\infty}\int_{-\infty}^{\infty}F(x,\tau)\exp(-i\Omega\tau + i\xi x)\mathrm{d}x\mathrm{d}\tau. \tag{36}$$

The temporal- and spatial-frequency domain coupled equations are

$$i\frac{\partial\hat{B}_1}{\partial\bar{z}} - \frac{L}{L'_{D,1}}\bar{\Omega}_1^2\hat{B}_1 + \gamma_1\frac{L}{L_{R,1}}\bar{\Omega}_1\bar{\xi}_1\hat{B}_1 = 0, \tag{37}$$

$$i\frac{\partial \hat{B}_2}{\partial \bar{z}} + \frac{L}{L_a}\bar{\xi}_2\hat{B}_2 - \frac{L}{L'_{D,2}}\bar{\Omega}_2^2\hat{B}_2 + \gamma_1\frac{L}{L_{R,2}}\bar{\Omega}_2\bar{\xi}_2\hat{B}_2 = c_2\hat{F}_2(z,\bar{\xi}_2,\bar{\Omega}_2), \tag{38}$$

where $\bar{\Omega}_i = \tau_0(\omega - \omega_i)$ is the normalized frequency detuning and $\bar{\xi}_i = w_0(k_x - k_{x,i})$ is the normalized spatial-frequency detuning. The transform of the square of the FH field envelope is written as the self-convolution of the transform of the FH envelope:

$$\hat{F}_2(\bar{z},\bar{\xi}_2,\bar{\Omega}_2) = \frac{1}{2\pi}\int_{-\infty}^{\infty}\int_{-\infty}^{\infty}\hat{B}_1(\bar{z},\bar{\xi}',\bar{\Omega}')\hat{B}_1(\bar{z},\bar{\xi}_2 - \bar{\xi}',\bar{\Omega}_2 - \bar{\Omega}')\mathrm{d}\bar{\xi}'\mathrm{d}\bar{\Omega}'. \tag{39}$$

The solution to Eq. (37) is

$$\hat{B}_1(\bar{z},\bar{\xi}_1,\bar{\Omega}_1) = \hat{B}_0(\bar{\xi}_1,\bar{\Omega}_1)\exp\left[-i\left(\frac{L}{L'_{D,1}}\bar{\Omega}_1^2 - \gamma_1\frac{L}{L_{R,1}}\bar{\Omega}_1\bar{\xi}_1\right)\bar{z}\right], \tag{40}$$

where $\hat{B}_0(\bar{\xi}_1,\bar{\Omega}_1)$ is the input FH field envelope, defined at $\bar{z}=0$. We define the input FH envelope at $\bar{z}=0$ in the center of the crystal, instead of at the incident face ($\bar{z}=-1/2$) since the former is typically the location where the dispersed field is reimaged from the diffraction grating and where the effective GVD due to pulse-front dispersion is arranged to vanish. Of course, the total effective GVD is only zero at this point if material GVD may be ignored; so in the case where material GVD is nonnegligible, one must take care to include the material GVD from the first half of the nonlinear crystal into this definition of the field envelope.

According to Eq. (40), the spectral amplitude of the FH field does not change, consistent with the assumption of an undepleted pump, but it acquires a spectral phase resulting from effective dispersion and spectral angular dispersion. To obtain the solution for the SH, it is convenient to define

$$\hat{G}_2(\bar{z},\bar{\xi}_2,\bar{\Omega}_2) = \hat{B}_2(\bar{z},\bar{\xi}_2,\bar{\Omega}_2)\times\exp\left[-i\left(\frac{L}{L_a}\bar{\xi}_2 - \frac{L}{L'_{D,2}}\bar{\Omega}_2^2 + \gamma_1\frac{L}{L_{R,2}}\bar{\Omega}_2\bar{\xi}_2\right)\bar{z}\right]. \tag{41}$$

The field $\hat{G}_2$ has the same spectral amplitude as $\hat{B}_2$, but explicitly factors out the spectral phase of a freely propagating SH field so that we can more clearly see the effects of frequency conversion.

We find on substitution of the definition in Eq. (41) into Eq. (38) that the solution for the field $\hat{G}_2(\bar{z},\bar{\xi}_2,\bar{\Omega}_2)$ is

$$\hat{G}_2(\bar{z},\bar{\xi}_2,\bar{\Omega}_2) = \int_{-1/2}^{1/2} -ic_2\hat{F}_2(z,\bar{\xi}_2,\bar{\Omega}_2)\times\exp\left[-i\left(\frac{L}{L_a}\bar{\xi}_2 - \frac{L}{L'_{D,2}}\bar{\Omega}_2^2 + \gamma_1\frac{L}{L_{R,2}}\bar{\Omega}_2\bar{\xi}_2\right)\bar{z}\right]\mathrm{d}\bar{z}. \tag{42}$$

The limits of integration indicate that the interaction occurs over $-L/2 \leqslant z \leqslant L/2$. Equation (42), along with the definitions in Eqs. (39) and (41) and the FH solution in Eq. (40), represents the solution for broadband SHG of a tilted FH field with angular dispersion characterized by γ_1.

7. SOLUTION FOR A GAUSSIAN FIRST-HARMONIC FIELD ENVELOPE

Equation (42) is a general solution for tilted pulse SHG, but in its current form is not particularly instructive. We can evaluate this expression in the particular case of a Gaussian FH input field; the resulting SH field expression will give insight into the behavior of a tilted pulse-front SHG. We define an initial FH field envelope

$$B_0(\bar{x},\bar{\tau}) = \exp\left(-\frac{\bar{x}^2}{2} - \frac{\bar{\tau}^2}{2}\right), \tag{43}$$

where the characteristic beam size w_0 and pulse width τ_0 are defined as $1/e$ intensity half-widths of the field envelope $B_0(x,\tau)$. Using the transform pair in Eqs. (35) and (36), the frequency and spatial-frequency domain FH field envelope is

$$\hat{B}_0(\bar{\xi}_1,\bar{\Omega}_1) = \exp\left(-\frac{\bar{\xi}_1^2}{2} - \frac{\bar{\Omega}_1^2}{2}\right). \tag{44}$$

Substituting this Gaussian field into Eq. (40) we can compute $\hat{F}_2(z,\bar{\xi}_2,\bar{\Omega}_2)$ using Eq. (39) to find

$$\hat{F}_2(\bar{z},\bar{\xi}_2,\bar{\Omega}_2) = \frac{1}{2\left[1 + 2i\frac{L}{L'_{D,1}}\bar{z} + \gamma_1^2\left(\frac{L}{L_{R,1}}\right)^2\bar{z}^2\right]^{1/2}}\times\exp\left[-\frac{\bar{\Omega}_2^2}{4}\left(1 + 2i\frac{L}{L'_{D,1}}\bar{z}\right) - \frac{\bar{\xi}_2^2}{4} + i\gamma_1\frac{L}{L_{R,1}}\frac{\bar{\Omega}_2\bar{\xi}_2\bar{z}}{2}\right]. \tag{45}$$

Substituting Eq. (45) into Eq. (42), we find an expression for the output field envelope $\hat{G}_2$, related to $\hat{B}_2$ through Eq. (41):

$$\hat{G}_2(\bar{z}=1/2,\bar{\xi}_2,\bar{\Omega}_2) = \frac{-ic_2}{2}\exp\left(-\frac{\bar{\Omega}_2^2}{4} - \frac{\bar{\xi}_2^2}{4}\right)I_2(q), \tag{46}$$

where

$$I_2(q) = \int_{-1/2}^{1/2}\frac{\exp(iqz)}{\left[1 + 2i\frac{L}{L'_{D,1}}z + \gamma_1^2\left(\frac{L}{L_{R,1}}\right)^2 z^2\right]^{1/2}}\mathrm{d}z, \tag{47}$$

$$q = \gamma_1\delta_R\bar{\Omega}_2\bar{\xi}_2 + \delta_D\bar{\Omega}_2^2 - A\bar{\xi}_2. \tag{48}$$

The first term in the expression for q represents mismatch in the spectral angular dispersion between FH and SH fields, where we define

$$\delta_R = \frac{1}{2}\frac{L}{L_{R,1}} - \frac{L}{L_{R,2}} = \frac{L}{w_0^2 k_1 k_2}(k_2 - 2k_1). \tag{49}$$

Although we have assumed that the FH and SH angular dispersion is equal to that required to maintain phase matching across the bandwidth of our short pulse, according to the conditions given in Eqs. (2) and (4), dispersion in the refractive index causes these two waves to disperse differently as their frequency components separate in space. The first term in q reflects the mismatch in angular dispersion and is equal to zero if there is no angular dispersion $\gamma_1 = 0$ or if there is no difference in the refractive index at the FH and SH waves $n_1 - n_2 = 0$.

The second term represents mismatch in effective GVD:

$$\delta_D = \left(\frac{L}{L'_{D,2}} - \frac{1}{2}\frac{L}{L'_{D,1}}\right) = \frac{L}{2\tau_0^2}\left(\beta_2 - \frac{\beta_1}{2}\right) + \frac{\gamma_1^2 L}{2w_0^2 k_1 k_2}(2k_1 - k_2). \tag{50}$$

The first part is the mismatch in material GVD, and the second part represents the mismatch in effective GVD that arises from the diffraction of a strongly tilted pulse. Depending on the geometry, the total effective GVD may be dominated by either effect, but we note that the effective dispersion term is of the order of γ_1 larger than the angular dispersion effect in Eq. (49), so the angular dispersion mismatch may be ignored in the limit $|\gamma_1| \gg 1$. The third term in q represents the effects of spatial walk-off with the parameter A defined as the ratio

$$A = \frac{L}{L_a}. \tag{51}$$

The behavior of SHG in the presence of spectral angular dispersion depends centrally on the evaluation of $I_2(q)$, which represents the influence of spatial walk-off and GVD and can affect both the amplitude and the shape of the SH envelope. The parameter q includes all frequency and spatial-frequency dependence and groups together the effects of angular dispersion mismatch, effective GVD mismatch, and spatial walk-off. To determine the magnitude of these effects, we need only to examine each of the terms in the expression for q and evaluate the dependence of $I_2(q)$ on q.

We can evaluate $I_2(q)$ in some practical limits that simplify the mathematics but still reveal clearly the essential physics. The first approximation is to assume strong spectral angular dispersion, or $|\gamma_1| \gg 1$. In addition, we assume that $\gamma_1^2 \gg 2L_R/L_D$, or equivalently, that the effective GVD is dominated by diffractive effects instead of material GVD and, according to Eq. (33), $L'_{D,1} \approx -2L_{R,1}/\gamma_1^2$. With these simplifications,

$$I_2(q) = \int_{-1/2}^{1/2} \frac{\exp(iqz)}{(1 - 2iDz)^{1/2}} \mathrm{d}z, \tag{52}$$

where we defined the ratio $D = -L/L'_{D,1} \approx \gamma_1^2 L/2L_{R,1}$ to simplify the notation. Since q is a function of $\bar{\Omega}$ and $\bar{\xi}$, $I_2(q=0)$ represents the value at $\bar{\Omega}=0$ and $\bar{\xi}=0$, or the midband amplitude reduction. At the midband, the integral can be readily evaluated, and we define this midband amplitude as $I_0(D)$:

$$I_0(D) = I_2(q=0) = 2\mathcal{I}\left[\frac{1}{D}(1 - iD)^{1/2}\right], \tag{53}$$

where $\mathcal{I}(x)$ denotes the imaginary part of x. This function is plotted in Fig. 6. When $D \ll 1$, $I_0 \approx 1$ and the midband SH amplitude is not influenced by the effective GVD. If $D \gg 1$, $I_0 \approx (2/D)^{1/2}$ and the midband SH amplitude decreases with an increasing ratio of $|L/L'_{D,1}|$.

In the general case the integral in Eq. (52) cannot be expressed in terms of elementary functions, but may be expressed in terms of the complex error function defined as

$$\mathrm{erf}(z) = \frac{2}{\sqrt{\pi}}\int_0^z \exp(-u^2)\mathrm{d}u, \tag{54}$$

and $I_2(q)$ is given by

$$I_2(q) = \mathrm{sgn}(q)\exp\left(\frac{q}{2D}\right)\mathcal{I}\left\{\left(\frac{2\pi}{qD}\right)^{1/2}\mathrm{erf}\left[\frac{q}{2}\left(\frac{1}{D} - i\right)\right]^{1/2}\right\}, \tag{55}$$

where $\mathrm{sgn}(q) = q/|q|$.

In Fig. 7 we show a few cases of $I_2(q)$ for different values of D, including the limiting cases of $D \gg 1$ and $D \ll 1$.

When $D \ll 1$,

$$I_2(q) \approx \mathrm{sinc}(q/2), \tag{56}$$

where $\mathrm{sinc}(x) = \sin(x)/x$. When $D \gg 1$, $I_2(q)$ has the approximate solution

$$I_2(q) = \mathrm{sgn}(q)\left(\frac{2}{D}\right)^{1/2}\mathcal{I}\left[\left(\frac{\pi}{q}\right)^{1/2}\mathrm{erf}\left(\frac{-iq}{2}\right)^{1/2}\right]. \tag{57}$$

In this limit, only the amplitude and not the shape of $I_2(q)$ is influenced by the value of D.

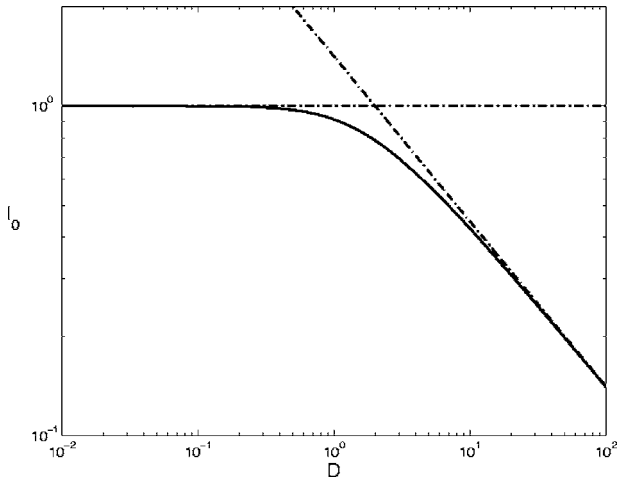

Fig. 6. SH amplitude reduction $I_0(D)$. The solid curve is $I_0(D)$, and the dashed–dotted lines indicate asymptotic behavior for $D \ll 1$ where $I_0(D) \approx 1$ and $D \gg 1$ where $I_0(D) \approx \sqrt{2/D}$.

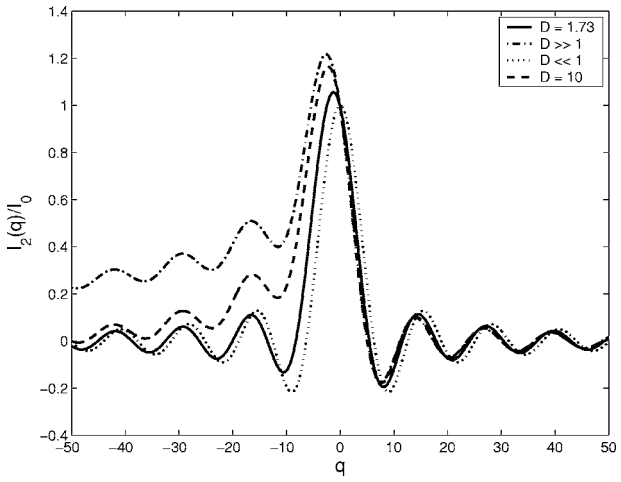

Fig. 7. Evaluation of the response function $I_2(q)$ for several values of D, normalized to the value at $q=0$. When $D \ll 1, I_2(q) \approx \mathrm{sinc}(q/2)$. When $D \gg 1, I_2(q)$ is asymmetric with a slowly decaying tail.

8. EFFECTS OF GROUP-VELOCITY DISPERSION AND SPATIAL WALK-OFF

Spatial walk-off and GVD are important effects influencing the behavior of SHG. In their absence, $I_2(q)=1$ and the solution for tilted pulse-front SHG in Eq. (46) is trivial. The magnitudes of these effects are set by the magnitudes of the constants in Eqs. (49) through (51). These constants depend not only on material parameters, but on experimental conditions (i.e., interaction length, beam waist, pulse-front tilt) as well.

To understand the effect of spatial walk-off and GVD on conversion efficiency, bandwidth, and beam shape, we investigate the influence of these effects on the solution in Eq. (46). All frequency and spatial-frequency behavior is contained in $I_2(q)$, since q is a function of $\bar{\Omega}$ and $\bar{\xi}$.

The effect of GVD manifests itself in two forms. First, when the magnitude of dispersion at the fundamental frequency is large, the peak intensity decreases with propagation distance, reducing the effective interaction length. The magnitude of the FH dispersion appears in the ratio D and consequently affects the midband SH amplitude reduction in Eq. (53). This reduced efficiency is the result of a reduced peak FH intensity in the presence of dispersion. Since the magnitude of D does not directly affect the shape of $I_2(q)$, the frequency content of the SH field is not affected by the magnitude of the effective dispersion represented by D.

Although the magnitude of GVD does not directly affect the bandwidth of SHG, the mismatch between the effective dispersion of FH and SH fields (represented by the coefficient δ_D) may influence the SH frequency content. When the effective GVD of the FH polarization and the SH field are mismatched, the result is a phase mismatch that can accumulate across the bandwidth of a short optical pulse, limiting the bandwidth of the SHG interaction. If the largest term in q is the GVD term in Eq. (48), then $q \approx \delta_D \bar{\Omega}^2$ where δ_D is the effective GVD mismatch, defined in Eq. (50). The frequency-domain field envelope $\hat{G}_2$ is the product of I_2 and the transform of the square of the envelope of the FH field, as in Eq. (41). In Fig. 8 we show the bandwidth reduction versus δ_D for several values of D. With negligible dispersion mismatch ($|\delta_D| \ll 1$), the expected bandwidth is $\sqrt{2}$ times larger than the input FH bandwidth. The bandwidth decreases approximately as $|\delta_D|^{-1/2}$ for $|\delta_D| \gg 1$. To preserve the bandwidth of the SHG interaction, we should choose the interaction length, pulse-front tilt, and beam size such that $|\delta_D| \ll 1$.

Note that when $D \gg 1$, the bandwidth is asymmetric in δ_D and even exhibits a larger bandwidth than the $\delta_D=0$ case. This is due to the asymmetry in $I_2(q)$ for $D \gg 1$ shown in Fig. 7. Since q is quadratic in $\bar{\Omega}$, and the envelope of $I_2(q)$ is not symmetric in q, the behavior can be quite different for different signs of δ_D.

When q [see Eq. (48)] is dominated by the spatial walk-off term, $q \approx -A\bar{\xi}_2$, where $A=L/L_a$. In this limit, I_2 is independent of $\bar{\Omega}$; and even in the limit of large spatial walk-off, the frequency content of the electric field is unaltered. Walk-off will, however, limit the spatial-frequency content for large values of $|A|$ and accordingly affects the size and shape of the SH beam. Although negligible dispersion mismatch ($|\delta_D| < 1$) is a necessary condition for preserving the bandwidth of SHG, spatial walk-off does not affect the frequency bandwidth. In Fig. 9 we show the effects of varying spatial walk-off on the output beam size and shape for different values of the effective dispersion characterized by D. In all cases, as A increases, the beam size increases when $I_2(q=-A\bar{\xi}_2)$ becomes narrower than the field envelope, or when $|A| \approx 1$ and the field envelope is influenced by the shape of $I_2(q=-A\bar{\xi}_2)$. Although when $D \ll 1$ the resulting beam profile for $|A| \gg 1$ would be a top hat [i.e., with a Fourier transform proportional to $I_2(q)=\mathrm{sinc}(q/2)$, at larger values of D we can see this is not true. In Section 10 we discuss how the beam size and quality trade off against conversion efficiency.

In this section we have considered separately the influence of spatial walk-off and GVD mismatch. When one effect is clearly dominant it influences separately the frequency and spatial-frequency content of the SH envelope, i.e., spatial walk-off does not influence the frequency con-

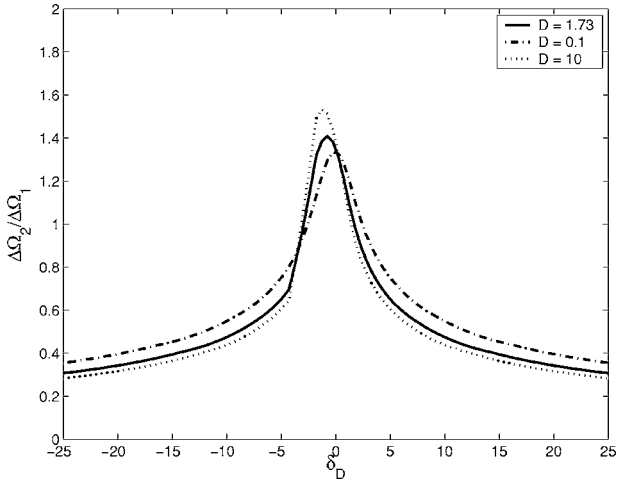

Fig. 8. SHG acceptance bandwidth versus effective GVD mismatch parameter δ_D defined in Eq. (50) for several values of the FH effective dispersion parameter D. Here we neglect spatial walk-off and assume that $q \approx \delta_D \Omega_2^2$. Minimal loss of bandwidth results when $|\delta_D| < 1$ regardless of the magnitude of D.

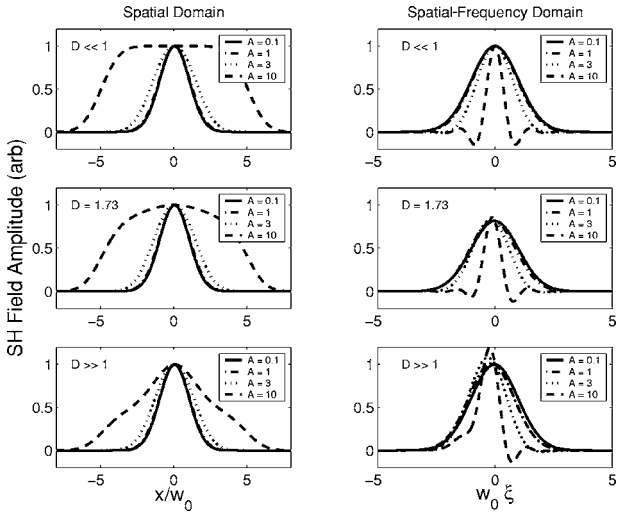

Fig. 9. Effects of spatial walk-off on beam profile for several values of the spatial walk-off parameter $A=L/L_a$. On the left is plotted the near-field SH amplitude versus x, and on the right the field amplitude versus spatial frequency (proportional to the far-field SH amplitude distribution after angular dispersion has been compensated) is shown. The shape of the response function $I_2(q)$ is influenced by the dispersion parameter D, while increasing A changes the scaling of the width of the response function in the spatial-frequency domain since $q=A\xi$. When $A \ll 1$, the response function is much wider than the polarization distribution, and both the near-field and far-field distributions are Gaussian for all values of D. When $A>1$, the response function is narrower than the polarization distribution, and the SH amplitude is influenced by the shape of $I_2(q)$. When $D \ll 1$ (top graphs), $I_2(q) \approx \mathrm{sinc}(q)$ and the near-field distribution approaches a flat-top function. For larger D (middle and bottom graphs), $I_2(q)$ departs from the sinc(q) behavior as shown in Fig. 7, and the near-field and far-field distributions reflect the distortion of the response function when $A>1$.

tent of the SH envelope, and GVD mismatch does not affect the SH spatial envelope. In general, however, q contains terms influenced by both spatial walk-off and GVD mismatch as shown in Eq. (48). If both L/L_a and δ_D are of comparable magnitude, they must be considered together in the evaluation of $I_2(q)$. Consequently the frequency and spatial-frequency behavior may not be separately attributed to the magnitude of GVD mismatch and spatial walk-off, respectively.

For the remainder of this paper, we assume that $|\delta_D| \ll 1$ so as to preserve the bandwidth of SHG, and the effects of GVD mismatch are neglected.

9. CONVERSION EFFICIENCY IN THE ABSENCE OF SPATIAL WALK-OFF AND GROUP VELOCITY DISPERSION

With the field solution of Eq. (46), we can compute the energy conversion efficiency for tilted pulse-front SHG as the ratio of SH energy to FH energy:

$$\eta = \frac{U_2}{U_1} = \frac{n_2}{n_1} \frac{\int_{-\infty}^{\infty}\int_{-\infty}^{\infty} |\hat{B}_2(\bar{z}=1/2,\bar{\xi},\bar{\Omega})|^2 \mathrm{d}\bar{\xi}\mathrm{d}\bar{\Omega}}{\int_{-\infty}^{\infty}\int_{-\infty}^{\infty} |\hat{B}_0(\bar{\xi},\bar{\Omega})|^2 \mathrm{d}\bar{\xi}\mathrm{d}\bar{\Omega}}. \quad (58)$$

We evaluate the conversion efficiency using the definition of $\hat{G}_2$ in Eq. (46), its relation to $\hat{B}_2$ in Eq. (41), and the FH field used in this Gaussian example from Eq. (44). In the limit of negligible effective GVD and angular dispersion, $I_2 \approx 1$. If we write c_2 [defined in Eq. (20)] in terms of the FH pulse energy,

$$c_2^2 = \frac{8\pi d_m^2}{\epsilon_0 c n_2^2 n_1 \lambda_1^2} \frac{U_1 L^2}{w_0 \sigma_y \tau_0}, \quad (59)$$

where σ_y is the effective cross section of the FH beam in the transverse y dimension (equal to $\sqrt{\pi} w_y$ for a Gaussian field). The conversion efficiency is

$$\eta_0 = \frac{n_2}{n_1}\frac{c_2^2}{2} = \frac{4\pi d_m^2}{\epsilon_0 c n_2 n_1^2 \lambda_1^2} \frac{U_1 L^2}{w_0 \sigma_y \tau_0}. \quad (60)$$

The conversion efficiency is equal to the well-known result for an untilted Gaussian FH pulse in the absence of GVM, GVD, diffraction, and spatial walk-off.[2] The peak power conversion efficiency is $n_2 c_2^2/n_1$, and an additional factor of 1/2 results from our averaging this peak power efficiency over Gaussian envelopes in the transverse x dimension and in time. Our theoretical model ignores variations in the field envelope in the transverse y dimension and consequently assumes an equal effective area of the FH and SH envelopes in this dimension. However, considering a Gaussian envelope in y simply involves substituting the FH effective area $\sigma_y = \sqrt{\pi} w_y$ and further reducing the expression in Eq. (60) by a factor of $1/\sqrt{2}$ due to the averaging of conversion efficiency over a Gaussian envelope in the y dimension. With such a substitution, Eq. (60) is equivalent to the plane-wave estimate in Eq. (7).

In the presence of GVM, if we choose our interaction length $L=2L_g$ to preserve the pulse width,[2] the conversion efficiency for an untilted Gaussian FH beam limited by GVM is

$$\eta_{\mathrm{GVM}} = \frac{38.3 d_m^2}{\epsilon_0 c n_2 n_1^2 \lambda_1^2} \frac{U_1 L_g^2}{w_0 \sigma_y \tau_0} = 3.05 \frac{L_g^2}{L^2} \eta_0, \quad (61)$$

and we find that using spectral angular dispersion gives an advantage of $0.33L^2/L_g^2$ in conversion efficiency over using a collinear geometry and a bandwidth-limited crystal length equal to $2L_g$. Using a chirped grating with an optimum grating chirp ($D_g = 3\delta\nu/\tau_0 L$) and an unchirped FH pulse, we obtain a conversion efficiency of[2]

$$\eta_{\mathrm{CG}} = 1.37 \frac{L}{L_g} \eta_{\mathrm{GVM}} = 4.18 \frac{L_g}{L} \eta_0, \quad (62)$$

and the efficiency for the spectral angular dispersion technique is greater by a factor of $0.24L/L_g$ than when we use a chirped QPM grating.

10. CONVERSION EFFICIENCY IN THE PRESENCE OF SPATIAL WALK-OFF AND GROUP-VELOCITY DISPERSION: OPTIMIZING THE FOCUSING CONDITIONS AND PHASE-MATCHING ANGLE

Although it is always possible through appropriate choice of the phase-matching angle and the beam size to design an experiment with negligible effective GVD and spatial walk-off, it is not true that those conditions result in the

peak conversion efficiency. Here we assume that the GVD mismatch parameter $\delta_D \ll 1$, so that $q=-A\bar{\xi}_2$ with $A=L/L_a$.

In designing an experiment we are free to choose the focusing conditions, and (in the absence of optical damage) there exists an optimum focusing condition for peak conversion efficiency. Boyd and Kleinman showed that, for cw interactions in the absence of spatial walk-off, there exists an optimum focusing condition approximated closely by confocal focusing, i.e., for a diffraction length equal to half of the crystal length.[25] The nature of this optimum condition involves a trade-off between high peak intensity and an effective interaction length that may be less than L for tightly focused beams. For beams with waists larger than the confocal waist, decreasing the waist results in an increased intensity that is approximately constant over the interaction length, and the result is higher conversion efficiency. For beams smaller than the confocal waist, however, the effective interaction length is reduced below the crystal length L and the conversion efficiency decreases with tighter focusing. An analagous qualitative argument may be made regarding the effective dispersion that exists in tilted pulse-front SHG, and below we will show that the maximum conversion efficiency is achieved when the interaction length is equal to 1.73 times the effective dispersion length. This result is analagous to the focusing condition for the best SHG conversion set forth in Ref. 25, where the interaction length is 2.84 times the FH confocal length. (This condition is often approximated by an interaction length equal to the confocal length, where the efficiency is 80% of the maxiumum but with a reduced peak intensity.)

In addition to a choice of focusing conditions, QPM affords us a choice of phase-matching angles if we can construct a QPM grating to phase match a variety of noncollinear interactions. Decreasing the phase-matching angle reduces spatial walk-off but also decreases the effective dispersion length (at a fixed spot size). Maximizing the conversion efficiency involves choosing properly both the focusing conditions and the phase-matching angle.

With a given nonlinear material at a fixed FH wavelength, the effective dispersion length $L'_{D,1}$ and the aperture length L_a are uniquely determined by the FH spot size w_0 and the phase-matching angle θ_0. Here we discuss what choice of L_a and $L'_{D,1}$, or equivalently w_0 and θ_0, leads to the maximum conversion efficiency of a particular interaction at a fixed interaction length.

Including the effects of spatial walk-off and effective dispersion,

$$\eta = \eta_0 h(D,A), \tag{63}$$

where η_0 is the conversion efficiency with negligible GVD and spatial walk-off, given in Eq. (60), and we define the efficiency reduction factor h as

$$h(D,A) = \frac{1}{2\pi}\int_{-\infty}^{\infty} |I_2(q)|^2 \exp\left(-\frac{\bar{\Omega}_2^2}{2}-\frac{\bar{\xi}_2^2}{2}\right) d\bar{\Omega}_2 d\bar{\xi}_2. \tag{64}$$

We recall the definition of parameters $A=L/L_a$ and $D=-L/L'_{D,1}$ representing the influence of spatial walk-off and effective dispersion, respectively. The efficiency reduction factor is plotted in Fig. 10 for several values of D. When $|A| \ll 1, h$ is simply the square of the amplitude reduction given in Eq. (53).

The efficiency reduction factor h is a function of D and A and is consequently also a function of both w_0 and θ_0. The coupling coefficient c_2 also changes with the input beam size, so maximizing the efficiency involves a balance between maximizing the reduction factor h and maximizing the coupling coefficient c_2.

We recall the definitions of the characteristic lengths L_a and $L'_{D,1}$ and rewrite c_2^2 from Eq. (59) as

$$c_2^2 = \frac{16\pi^{3/2} d_m^2 L_g}{\epsilon_0 c n_2^2 n_1^{1/2} \lambda_1^{5/2}} \frac{U_1 L^{1/2}}{\sigma_y \tau_0} \frac{L}{L_a}\left(\frac{L}{L'_{D,1}}\right)^{1/2}. \tag{65}$$

Upon substitution into Eq. (63), we find that the conversion efficiency is equal to

$$\eta = \frac{8\pi^{3/2} d_m^2 L_g}{\epsilon_0 c n_2 n_1^{3/2} \lambda_1^{5/2}} \frac{U_1 L^{1/2}}{\sigma_y \tau_0} A\sqrt{D} h(A,D). \tag{66}$$

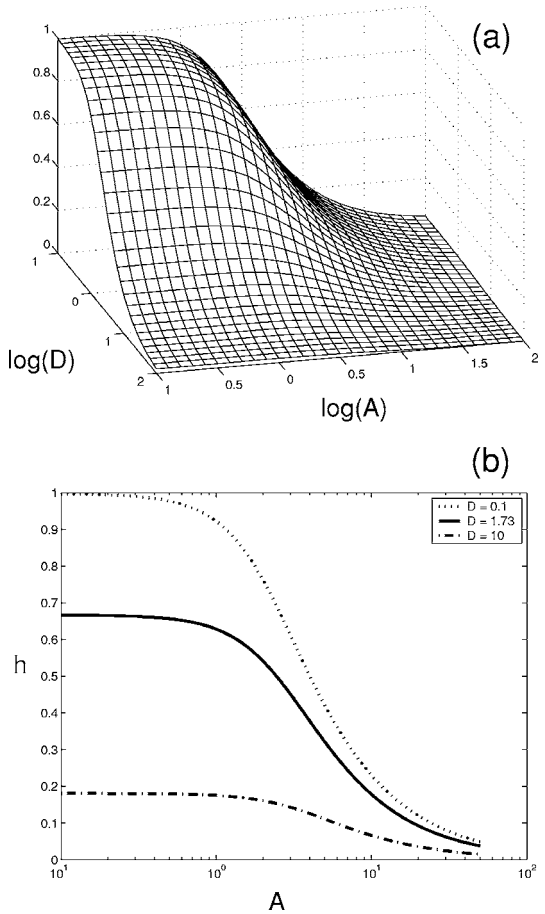

Fig. 10. (a) Surface plot of the efficiency reduction factor $h(A,D)$ as a function of $A=L/L_a$ and $D=L/L'_{D,1}$. When both spatial walk-off and effective dispersion are ignored ($A \ll 1$ and $D \ll 1$), $h(A,D) \approx 1$. Increased effective dispersion ($D>1$) leads to pulse spreading, and the length over which the intensity is at its maximum is reduced, resulting in a decreased conversion efficiency. Increased spatial walk-off ($A>1$) results in a generated SH field that propagates away from the peak FH intensity also resulting in a reduced effective interaction length and decreasing conversion efficiency. (b) Plot of $h(A,D)$ at fixed selected values of D. For $A \ll 1, h(A,D) \approx |I_0|^2$ as given in Eq. (53) determined only by the effective dispersion parameter D.

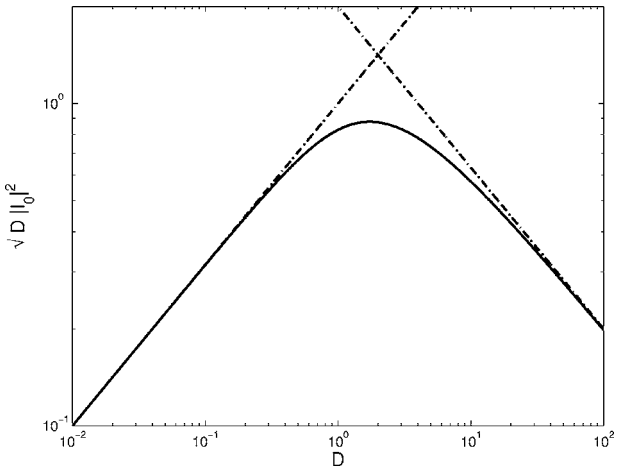

Fig. 11. Normalized SH amplitude is proportional to the function $\sqrt{D}|I_0(D)|^2$ and demonstrates a peak at $D=1.73$. The dashed–dotted lines indicate asymptotic behavior for $D \ll 1$ where $I_0(D) \approx 1$ and $D \gg 1$ where $I_0(D) \approx \sqrt{2/D}$.

At a fixed interaction length, variations in beam size w_0 and phase-matching angle θ_0 change only A and D, so that finding the maximum in $A\sqrt{D}h(A,D)$ will return the focusing and phase-matching conditions for peak conversion efficiency. A global optimization of the conversion efficiency predicts that the conversion efficiency saturates to its maximum value when A tends to infinity, i.e., the limit of large spatial walk-off corresponding to very tight focusing or a large phase-matching angle. Practically speaking, however, this results in an output SH envelope with a spatial-frequency distribution that is narrow (i.e., a wider SH beam) and resembles the function $I_2(q)$ shown in Fig. 7. The resulting beam profile may be a top hat when $D \ll 1$ and $I_2(q) \approx \mathrm{sinc}(q/2)$ or may have a spatial-frequency distribution with a slowly decaying asymmetric tail when $D \gg 1$.

Let us examine more closely the trade-off between beam quality and the conversion efficiency. When $A \ll 1$, $h = h_0 = |I_0(D)|^2$ and is independent of A. In Fig. 11 we plot $\sqrt{D}|I_0(D)|^2$, and it demonstrates a peak at $D_{\max} = 1.73$. This value of D maximizes the mid-spatial-frequency conversion efficiency. At larger values of D, the effective dispersion length is shorter than the interaction length, resulting in a decreased peak intensity over a significant portion of the interaction length. This decreased peak intensity is the source of the decreasing conversion efficiency when $D \gg 1$. For large pulse-front tilt $|\gamma_1| \gg 1$, we note that $D = 1.73$ implies $L/L_{R,1} \ll 1$, and the entire interaction takes place in the near field of the FH beam.

In the limits when $D \ll 1$ and $D \gg 1$, Eqs. (56) and (57) demonstrate that the value of D affects the amplitude of $I_2(q)$, but not the functional form. Indeed, even when $D \approx 1$, the shape of $I_2(q)$ changes very slowly with different values of D (see Fig. 7), and one might expect that the optimum value of D will be near its value when $A \ll 1$ for larger values of A. This assertion can be verified numerically; the optimum value for D is nearly independent of the choice of A. (For an absolute optimization of conversion efficiency, both D and A tend to infinity, but as we will show, a large A results in significant beam distortions. If reasonably good beam quality is desired, the optimum value for D can be treated independently of the choice of A.)

With an optimum value for D, we examine how the SH conversion changes by changing A with fixed D. With D fixed, the phase-matching angle is fixed, and changing $A = L/L_a = L\theta_0/w_0$ may be accomplished by changing the beam waist w_0. As A increases, the amplitude of the SH field increases as a result of the increased intensity resulting from a smaller beam waist, but the spatial-frequency bandwidth narrows as $I_2(q)$ becomes narrower than the Gaussian polarization envelope in Eq. (46). As a result, the SH beam broadens, and its shape is influenced by the shape of $I_2(q)$ as shown in Fig. 9. If $|A| \ll 1$, $I_2(q = -A\bar{\xi}_2)$ is approximately constant over the spatial-frequency envelope of $\hat{G}_2$, and the SH beam is Gaussian, with a beam quality parameter[26] $M^2 = 1$ and a beam size that is $\sqrt{2}$ times smaller than the FH pump beam.

Figure 12 quantifies the trade-offs between conversion efficiency and beam size and quality. Conversion efficiency, beam size, and beam quality are plotted as D is held fixed at its optimum value of $D_{\max} = 1.73$. When $A = 3$, the conversion efficiency is at 71% of its maximum value. The SH beam with $A = 3$ has a waist that is approximately $\sqrt{2}$ times larger than the $A \ll 1$ value, or roughly equal to the FH beam size w_0 and has $M^2 = 1.10$. (The beam quality parameter $M^2 = 1$ for a perfect Gaussian TEM_{00} mode and increases with increasing higher-order mode content. For a more complete discussion on the concept and measurement of M^2, see Ref. 26.) With $A = 3$ and $D = 1.73$, $h(A,D) = 0.45$ and the conversion efficiency in Eq. (66) is

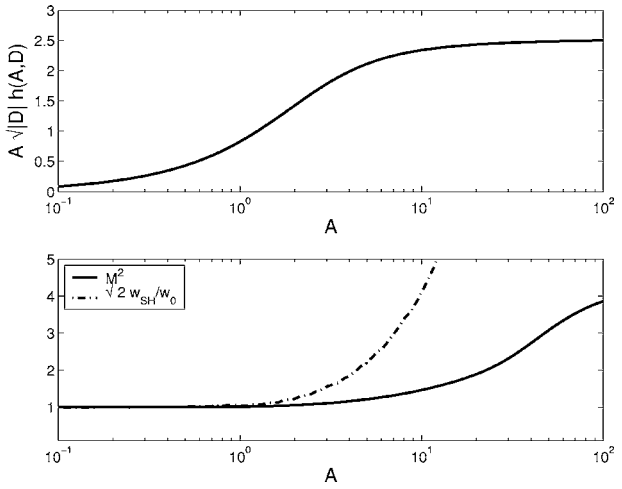

Fig. 12. Trade-off of normalized conversion efficiency (top) and beam size and quality (bottom) with optimum dispersion parameter $D = 1.73$ in the presence of spatial walk-off. At a fixed value of D, the spatial walk-off parameter $A = L/L_a$ is increased by decreasing the beam size w_0. The increased intensity results in higher conversion efficiency, but the resulting increase in spatial walk-off causes an increase in SH beam size and poor SH spatial mode quality. A compromise may be reached for $A \approx 3$, where the conversion efficiency reaches 71% of its maximum value, but the beam is approximately equal to the FH beam size with a beam quality parameter $M^2 = 1.10$ ($M^2 = 1$ implies a Gaussian TEM_{00} mode).

$$\eta = \frac{79 d_m^2}{\epsilon_0 c n_2 n_1^{3/2} \lambda_1^{5/2} \delta\nu} \frac{U_1 L^{1/2}}{\sigma_y}. \quad (67)$$

If we further presume that the beam is confocally focused in the transverse y (nondispersed) dimension for maximum conversion efficiency,[25] then $\sigma_y = (L\lambda_1/3.2n_1)^{1/2}$, and the optimized conversion efficiency is

$$\eta_{\mathrm{opt}} = \frac{141.4 d_m^2}{\epsilon_0 c\, \delta\nu n_2 n_1 \lambda_1^3} U_1. \quad (68)$$

We can compare this result with the conversion efficiency for collinear SHG in a uniform crystal with a bandwidth-limited length of $L = 2L_g$ and confocal focusing,[2]

$$\eta_{\mathrm{GVM}}^{\mathrm{conf}} = \frac{76.7 d_m^2}{\epsilon_0 c\, \delta\nu n_1 n_2 \lambda_1^3} U_1, \quad (69)$$

and with the conversion efficiency for collinear SHG in a chirped QPM grating with confocal focusing,[2]

$$\eta_{\mathrm{CG}}^{\mathrm{conf}} = 1.39\, \eta_{\mathrm{GVM}}^{\mathrm{conf}} = \frac{106.6 d_m^2}{\epsilon_0 c\, \delta\nu n_1 n_2 \lambda_1^3} U_1, \quad (70)$$

and we find that the scaling of the conversion efficiency for all three cases is identical. The difference in the magnitude of the conversion efficiency lies primarily in selecting the best conditions, since all three techniques require some subjective choice regarding a trade-off. Noncollinear SHG with spectral angular dispersion trades off beam quality with conversion efficiency, whereas the other two trade off bandwidth and conversion efficiency. In all three cases, a slightly higher conversion efficiency may be obtained at an expense of either decreased SH bandwidth or reduced SH beam quality.

Since all three techniques under optimum focusing conditions yield approximately identical values for energy conversion efficiency, other considerations may influence the experimenter's choice regarding the best method in a particular application. For example, using a short QPM grating is significantly simplier than using chirped gratings or spectral angular dispersion, as no dispersive elements are required. Dispersive elements are required when either a chirped QPM grating (a grating pair or dispersive material is required to compress the chirped SH output) or spectral angular dispersion is used (a grating or prism is required at the input to impose angular dispersion on the FH and at the output to compensate the angular dispersion of the generated SH field). Additional dispersive elements add both complexity and loss. However, since a short QPM grating is much shorter than the crystal length that may be used for the other two techniques, the required focusing for best conversion requires a much smaller spot size and results in a correspondingly high peak intensity. If this intensity exceeds the damage intensity, or leads to increased two-photon absorption, either of the other two techniques allows for the same conversion efficiency at much larger spot sizes. In the tilted pulse-front case, the optimum is reached when the beam size is larger than confocal and so offers a lower peak intensity for the same conversion as a chirped grating of equivalent crystal length. The peak FH intensity in noncollinear SHG with spectral angular dispersion under the optimum focusing conditions discussed above is a factor of $8(L_g/L)^2$ lower than the peak intensity for a short crystal of length $2L_g$ under confocal focusing conditions and is a factor of $4L_g/L$ lower than for confocal focusing into a chirped QPM crystal of equivalent length L.

If we now return to the experiment in Section 4, we can include the effective dispersion and spatial walk-off through the efficiency reduction factor $h(A,D)$ in Eq. (63). With a beam size $w_0 = 180$ μm and a phase-matching angle of $\theta_0 = 1.92$ deg, the aperture length is 5.6 mm, making $A = L/L_a = 1.8$ for a crystal length of 1 cm. The group-velocity walk-off length L_g is equal to 260 μm for our 138 fs pulses ($\tau_0 = 84$ fs), so that the pulse-front tilt parameter $|\gamma_1| = L_a/L_g = 21$ and the effective dispersion length is $|L'_{D,1}| = 1.4$ mm with $D = 7.1$. The GVD mismatch parameter $\delta_D = 0.31$, so we expect negligible loss of bandwidth. The corresponding efficiency reduction factor $h(A,D)$ is 21%, making the calculated conversion efficiency 14.7%, which is in reasonable agreement with the observed 6.7%. We note that these values of A and D are not the optimum values computed in our theoretical calculation, and accordingly with our 1 cm length crystal we could achieve a higher conversion efficiency by decreasing both the phase-matching angle and the beam size until $A \approx 3$ and $D = 1.73$, i.e., for $\theta_0 = 1.56$ deg and $w_0 = 91$ μm. With confocal focusing in the nondispersed dimension, the peak conversion efficiency calculated with Eq. (68) is 143%/nJ, or well into pump depletion with our FH pulse energy of 0.58 nJ.

11. CONCLUSION

We demonstrate frequency doubling of ultrashort pulses using spectral angular dispersion and a noncollinear geometry to eliminate the effects of GVM. Our experiment demonstrates SHG of pulses 138 fs in duration at a FH wavelength of 1550 nm in a PPLN crystal many times longer than the group-velocity walk-off length with negligible loss of SHG bandwidth.

In addition, we develop a theoretical model for group-velocity-matched SHG in quasi-phase-matched materials that includes the effects of dispersion, diffraction, and spatial walk-off. The diffraction of a strongly tilted pulse is treated as an effective dispersion, and a solution for the output SH field envelope is presented for the case of a Gaussian FH pump pulse. The diffraction of a strongly tilted pulse envelope is separated into the diffraction of the beam and an effective dispersion that results from the pulse-front tilt. The SH bandwidth may be limited by mismatch in the GVD or in the effective dispersion resulting from the diffraction of a tilted pulse. This total effective dispersion mismatch is characterized by a dispersion mismatch parameter δ_D, which should be less than unity to preserve the bandwidth of SHG. If $\delta_D \ll 1$, spatial walk-off and dispersion do not affect the frequency content of SHG and affect only the amplitude or beam shape.

The effective dispersion resulting from a tilted pulse front, combined with the effects of spatial walk-off, results in a reduced conversion efficiency characterized by an efficiency reduction factor. The efficiency reduction factor affects the optimum focusing condition and phase-

matching angle for peak conversion efficiency. This optimum is found where the phase-matching angle, inversely proportional to the pulse-front tilt, is chosen such that the effective dispersion resulting from the diffraction of a titled pulse has a characteristic length equal to 0.58 times the interaction length. In addition, the beam size is chosen to balance the trade-off between increasing conversion efficiency and increased distortions in the beam shape and quality due to spatial walk-off. A reasonable balance is found when the aperture length is approximately 1/3 the interaction length.

The best achievable conversion efficiency for noncollinear SHG with spectral angular dispersion is independent of the interaction length and is approximately equal to the conversion efficiency for other methods of ultrashort-pulse SHG under ideal focusing conditions.

ACKNOWLEDGMENTS

This research was funded by the U.S. Air Force Office of Scientific Research under contract F49620-02-1-0240. The authors are also grateful for generous donations of equipment and materials from Spectra-Physics Lasers and Crystal Technology, Inc.

REFERENCES

1. M. M. Fejer, G. A. Magel, D. H. Jundt, and R. L. Byer, "Quasi-phase-matched second harmonic generation: tuning and tolerances," IEEE J. Quantum Electron. **28**, 2631–2654 (1992).
2. G. Imeshev, M. A. Arbore, M. M. Fejer, A. Galvanauskas, M. Fermann, and D. Harter, "Ultrashort-pulse second-harmonic generation with longitudinally nonuniform quasi-phase-matching gratings: pulse compression and shaping," J. Opt. Soc. Am. B **17**, 304–318 (2000).
3. D. H. Jundt, "Temperature-dependent Sellmeier equation for the index of refraction, n_e, in congruent lithium niobate," Opt. Lett. **22**, 1553–1555 (1997).
4. M. S. Webb, D. Eimerl, and S. P. Velsko, "Wavelength insensitive phase-matched second-harmonic generation in partially deuterated KDP," J. Opt. Soc. Am. B **9**, 1118–1127 (1992).
5. K. Hayata and M. Koshiba, "Group-velocity-matched second-harmonic generation: an efficient scheme for femtosecond ultraviolet pulse generation in periodically domain-inverted β–BaB_2O_4," Appl. Phys. Lett. **62** 2188–2190 (1993).
6. N. E. Yu, J. H. Ro, M. Cha, S. Kurimura, and T. Taira, "Broadband quasi-phase-matched second-harmonic generation in MgO-doped periodically poled $LiNbO_3$ at the communications band," Opt. Lett. **27**, 1046–1048 (2002).
7. N. E. Yu, S. Kurimura, and K. Kitamura, "Broadband second harmonic generation with simultaneous group-velocity matching and quasi-phase matching," Jpn. J. Appl. Phys. Part 1 **42**, L821–L823 (2003).
8. N. E. Yu, S. Kurimura, K. Kitamura, J. H. Ro, M. Cha, S. Ashihara, T. Shimura, K. Kuroda, and T. Taira, "Efficient frequency doubling of a femtosecond pulse with simultaneous group-velocity matching and quasi phase matching in periodically poled, MgO-doped lithium niobate," Appl. Phys. Lett. **82**, 3388–3390 (2003).
9. H. Zhu, T. Wang, W. Zheng, P. Yuan, L. Qian, and D. Fan, "Efficient second harmonic generation of femtosecond laser at 1 μm," Opt. Express **12**, 2150–2155 (2004).
10. M. L. Bortz, M. Fujimura, and M. M. Fejer, "Increased acceptance bandwidth for quasi-phase-matched second harmonic generation in $LiNbO_3$ waveguides," Electron. Lett. **30**, 34–35 (1994).
11. M. A. Arbore, O. Marco, and M. M. Fejer, "Pulse compression during second-harmonic generation in aperiodic quasi-phase-matching gratings," Opt. Lett. **22**, 865–867 (1997).
12. V. D. Volosov, S. G. Karpenko, N. E. Kornienko, and V. L. Strizhevskii, "Method for compensating the phase-matching dispersion in nonlinear optics," Sov. J. Quantum Electron. **4**, 1090–1098 (1975).
13. V. D. Volosov and E. V. Goryachkina, "Compensation of phase-matching dispersion in generation of nonmonochromatic radiation harmonics. I. Doubling of neodymium-glass radiation frequency under free-oscillation conditions," Sov. J. Quantum Electron. **6**, 854–857 (1976).
14. S. Saikan, "Automatically tunable second-harmonic generation of dye lasers," Opt. Commun. **18**, 439–443 (1976).
15. O. E. Martinez, "Achromatic phase matching for second harmonic generation of femtosecond pulses," IEEE J. Quantum Electron. **25**, 2464–2468 (1989).
16. G. Szabo and Z. Bor, "Broadband frequency doubler for femtosecond pulses," Appl. Phys. B **50**, 51–54 (1990).
17. A. V. Smith, "Group-velocity-matched three-wave mixing in birefringent crystals," Opt. Lett. **26**, 719–721 (2001).
18. T. R. Zhang, H. R. Choo, and M. C. Downer, "Phase and group velocity matching for second harmonic generation of femtosecond pulses," Appl. Opt. **29**, 3927–3933 (1990).
19. S. Saikan, D. Ouw, and F. P. Schafer, "Automatic phase-matched frequency-doubling system for the 240–350-nm region," Appl. Opt. **18**, 193–196 (1979).
20. B. A. Richman, S. E. Bisson, R. Trebino, E. Sidick, and A. Jacobsen, "All-prism achromatic phase matching for second-harmonic generation," Appl. Opt. **38**, 3316–3323 (1999).
21. P. Baum, S. Lochbrunner, and E. Riedle, "Tunable sub-10-fs ultraviolet pulses generated by achromatic frequency doubling," Opt. Lett. **29**, 1686–1688 (2004).
22. M. Aoyama, T. Zhang, M. Tsukakoshi, and K. Yamakawa, "Noncollinear second-harmonic generation with compensation of phase mismatch by controlling frequency chirp and tilted pulse fronts of femtosecond laser pulses," Jpn. J. Appl. Phys. Part 1 **39**, 3394–3399 (2000).
23. S. Ashihara, T. Shimura, and K. Kuroda, "Group-velocity matched second-harmonic generation in tilted quasi-phase-matched gratings," J. Opt. Soc. Am. B **20**, 853–856 (2003).
24. S. A. Akhmanov, V. A. Vysloukh, and A. S. Chirkin, *Optics of Femtosecond Laser Pulses* (American Institute of Physics, 1992).
25. G. D. Boyd and D. A. Kleinman, "Parametric interactions of focused Gaussian light beams," J. Appl. Phys. **39**, 3597–3639 (1968).
26. T. F. Johnson, "Beam propagation (M^2) measurement made as easy as it gets: the four-cuts method," Appl. Opt. **37**, 4840–4850 (1998).